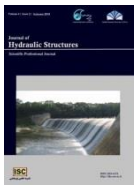
Journal of Hydraulic Structures
J. Hydraul. Struct., 2025; 11(1): 89-110
DOI: 10.22055/jhs.2024.47326.1307



OPEN ACCESS

Integrating Fuzzy Logic and Numerical Modeling for Analyzing Wave Patterns: A Study of the Makran Coastline

Maryam Rahbani[1]
Danial Ghaderi [2*]

Abstract

The Makran coastline, a strategic maritime region, has remained understudied regarding its hydrodynamic behavior. This study applies numerical simulations to analyze wave patterns in the northern Gulf of Oman, focusing on wave height (H_S), power (P), and mean wave direction (MWD) through Fuzzy Logic transformation and overlaying techniques. Seasonal and annual variations reveal that H_S ranges from 0.07 to 1.9 m, peaking during the summer with an average of 0.7 m, while winter and spring exhibit calmer conditions with an average H_S of 0.4 m. Wave power (P) shows a marked increase in summer, reaching up to 10.2 kW/m, with an annual mean ranging from 0.02 to 5.3 kW/m. Wave direction shifts seasonally, predominantly from 171° to 247° during winter and spring, and between 189° to 191° in summer and autumn. Spatial analysis highlights intensified hydrodynamic activity in the eastern region, influenced by oceanic conditions and the monsoon, while the western sector remains relatively calmer. Omega-shaped coasts and bays demonstrate more stable conditions, whereas headlands and capes experience significant hydrodynamic intensification. These findings provide critical insights for coastal management and sustainable development, enabling policymakers to balance maritime potential with risk mitigation. By integrating hydrodynamic dynamics into coastal planning, resilient strategies can be established for the sustainable utilization of the Makran region's resources.

Keywords: Makran; Gulf of Oman; Significant Wave Height; Wave Power; MIKE 21.

Received: 03 July 2024; Accepted: 11 September 2024

1. Introduction

The coastline has perpetually captivated human societies, serving as a focal area for settlement and development. Over 40% of the global population resides within 100 km of the coast [1], driven by factors such as food security, ocean transportation, and favorable climatic conditions [2,3].

*Email: danialghaderi.phd@hormozgan.ac.ir, danialghaderi1@gmail.com
[1] Department of Atmospheric and Oceanographic Science, Faculty of Marine Science and Technology, University of Hormozgan, Bandar Abbas, Iran.
[2] Researcher at Center Providing Consultation And Simulation Services For Coastal And Marine Environments (NPDS Company), Bandar Abbas, Iran.

However, these regions face significant challenges, such as coastal erosion and inundation [4,5]. These challenges, often driven by weather patterns and hydrodynamic behaviors in seas and oceans, pose serious threats to coastal human settlements [6,7]. Understanding the hydrodynamic conditions of coastal regions, as well as the morphological responses of shorelines to these conditions, is essential for effective coastal development [8].

One of the key regions where such an understanding is required is the west part of the Makran coast. This coastal area, located in the northern Gulf of Oman, is characterized by its dry and windy conditions, with limited rainfall and the presence of several seasonal rivers [9]. Despite some human settlements, this region remains sparsely populated. Development plans, however, have designated this coastal region for significant marine development, increasing the need to understand its hydrodynamic patterns. Therefore, the objective of this study is to analyze the patterns of hydrodynamic variables along this coastline, with a focus on integrating them using Fuzzy Logic techniques.

Some investigation of hydrodynamic conditions had been conducted in the coastal and offshore area of the northern Gulf of Oman through numerical simulation studies. For instance, Allahdadi et al., [10] utilized the MIKE 21 Spectral Waves (SW) to simulate the waves due to the Cyclone Gonu in June 2007 in the Gulf of Oman. The model was calibrated using data from the Chabahar buoy. The numerical model was used to analyze the behavior of Cyclone Gonu, starting from its formation in the Arabian Sea. In another research, utilizing the coupled models MIKE 21 SW and MIKE 21 hydrodynamic (HD), Moghaddam et al., [11] examined the local wave and wave-induced currents in Ramin Port, located in the northern part of the Gulf of Oman. The primary objective of utilizing the model was to find solutions for the sedimentation issues occurring within the port basins. The model encompasses both regional and offshore domains and has been validated using data from the Chabahar buoy. In order to examine the effects of constructing Beris port in the northern Gulf of Oman, Sayehbani and Ghaderi, [12] conducted a study on the hydrodynamic conditions of the area. They compared the conditions before and after the construction of the breakwater, focusing on the months of July and August when wind activity is quite strong. To analyze the wave pattern and current behavior near the port and its potential impact on sedimentation, they utilized the MIKE 21 SW and MIKE 21 HD models. In continuation of the studies on the impact of the construction of Beris Port, Ghaderi and Rahbani, [13] conducted a simultaneous investigation using hydrodynamical simulation and remote sensing (RS) imagery. They expanded the spatial and temporal range of their study to analyze the wave and current patterns as well as long-term shoreline changes. For the hydrodynamical study, they utilized the MIKE 21 Coupled model, ECMWF wind and wave data, and Chabahar buoy wave data. The findings of their study highlight the sedimentation problems faced by the port and its surrounding beaches. Armanfar et al., [14] utilized climate change scenarios to evaluate the vulnerability of the coastal areas in the Chabahar region (in the northeast part of the Gulf of Oman). They employed MIKE 21 numerical modeling to simulate the potential impacts of sea level rise, changes in significant wave height, and alterations in tidal patterns. The assessment focused on estimating possible changes until the year 2100. The findings indicated that a significant portion of the coastal zones in the Chabahar area face the risk of inundation due to sea storms and potential climate change. Siahsarani et al., [15] conducted a study focused on the analysis of Cyclone Gonu behavior and its impact on the storm surge in the Gulf of Oman. They conducted a numerical simulation that involved coupling wave and hydrodynamic models, specifically using MIKE 21 SW and MIKE 3 HD, along with measured data. The aim of the study was to investigate the role of variables in the model setup and their influence on coastal areas while studying the behavior of Cyclone Gonu. Foroutani et al., [16] investigated Tropical Cyclone Ashobaa in the Gulf of Oman

through numerical simulation. Their findings indicated that during storm conditions, there are substantial changes in water level, current speed, and even current direction in the Chabahar region.

While previous studies have provided valuable insights into the hydrodynamics of specific events or locations, none have offered a comprehensive assessment of wave patterns across the entire Makran coast. This study aims to fill this gap by using numerical simulations to analyze the spatiotemporal behavior of hydrodynamic variables along the Makran coastline, specifically focusing on wave height, wave power, and wave direction. The novelty of this research lies in the detailed analysis of wave patterns with sufficient accuracy to support coastal development projects in the region. To gain a comprehensive understanding of the hydrodynamic conditions, variables such as wave height (H_S), power (P), and mean wave direction (MWD) are integrated using Fuzzy Logic techniques. This approach allows for a more realistic description of the hydrodynamic environment, representing a significant innovation in the study of coastal hydrodynamics. Furthermore, it provides a clearer assessment of the region's potential for sustainable development while mitigating hydrodynamic risks.

2. Method

2. Study Area

Makran coast stretches along the Gulf of Oman for approximately 550 km (Fig. 1) [17]. This region is receiving significant attention from politicians and administrators, as it has been identified as an area with great potential for maritime development [18]. The development of marine industries along this coastline is still in its early stages. There are still no large-scale industries or ports in the area, but they are included in future development plans. Due to its proximity to the Arabian Sea and Indian Ocean, the region is constantly influenced by the climatic conditions of the northern Indian Ocean and the monsoon [19,20]. Additionally, previous reports and studies have highlighted the region’s vulnerability to tsunamis [21,22] and rising sea levels [23]. Makran coastal region encompasses a variety of landforms, such as sand spits and barrier islands primarily located in the western part of the region (Codes 2, 5, 8-11 and 15 in Fig 1). Additionally, there are mangrove forests and estuaries in both the eastern and western areas (Codes 2, 8, 11, 15, 29 and 30 in Fig 1). High beaches and rocky coastline are spesifically the characteristics of eastern part (Codes 17, 23, 24, 26, and 28 in Fig 1). Human settlements can also be found in both the eastern and western parts (Codes 6, 23, 24, and 28 in Fig 1). There are only two notable ports, namely Jask (Codes 6 in Fig 1) and Chabahar port (Codes 23 in Fig 1), in the area. These ports are both large and significant in terms of their infrastructure and capacity. The offshore part of the Makran region is significantly deep, reaching up to 2500-3000 m (Fig 1 C). Given the geomorphological diversity of the Makran region, with its eastern part adjacent to oceanic waters and its western part more distant from oceanic influence, it is essential to conduct a precise analysis of the hydrodynamic conditions, taking into account these variations. This study aims to address this gap by providing a detailed examination of these hydrodynamic differences.

Despite the presence of several rivers, the area is generally characterized as dry and semi-arid, resulting in low water levels or complete dryness for most of the year. The majority of rainfall occurs during the winter season, specifically during the winter monsoon period [24]. The wind patterns in the eastern and western parts of the study area differs. In the western part, the prevailing wind direction is from the W and E, with wind speeds exceeding 6 m/s from the W and NW. In the eastern part however, the wind primarily blows from the SE, with a secondary direction of W-SW [13]. The maximum wind speed in the southeast direction reaches up to 8 m/s. Figure 1 shows the bathymetry of the region utilizing GEBCO, and local depth data. To enhance the dissemination

of the findings, 30 major cities/villages of the area are identified in the figure, labeled as numbers 1-30 (Table 1).

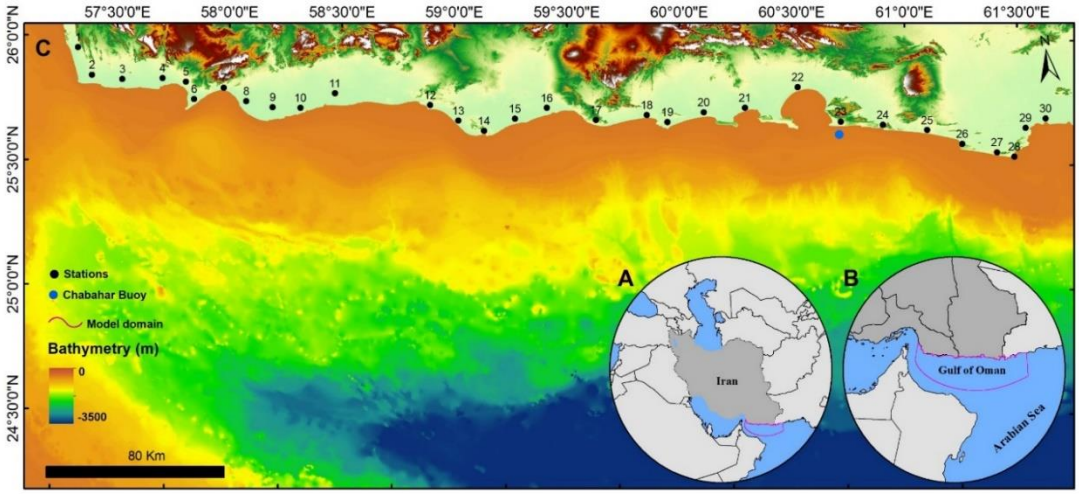


Figure 1. A & B) location of the study area, and C) Bathymetry of the area

Table 1. Location of zones in the study area

Zone	Name	Lat (°N) Long (°E)	Zone	Name	Lat (°N) Long (°E)	Zone	Name	Lat (°N) Long (°E)
1	Bunji-ye Karbasi	25.93048 57.31323	11	Gabrik & Jask Protected Area	25.64053 58.43555	21	Pozm Bay	25.39705 60.24757
2	Kuh Mobarak	25.81495 57.36336	12	Gougsar	25.55259 58.85217	22	Chabahar Bay	25.45441 60.49167
3	Gāvbandi	25.78589 57.49725	13	Lirak	25.47730 58.96959	23	Chahbahar	25.29404 60.66402
4	Rig	25.77291 57.67578	14	Kalirak	25.42460 59.07945	24	Lipār	25.26020 60.84942
5	Jāsk-e-kohne	25.74879 57.77878	15	Khowr Rapch	25.45963 59.22262	25	Rudik-e Molladad	25.21703 61.04211
6	Jask	25.67641 57.80693	16	Khowr Galak	25.48877 59.36922	26	Beris	25.14394 61.18974
7	Hojdān	25.70982 57.94357	17	Kalāt	25.41747 59.58070	27	Poshot	25.09217 61.33887
8	Shahreni	25.64608 58.03730	18	Birdaf	25.41375 59.80901	28	Pasabandar	25.06598 61.41234
9	Karap	25.61141 58.15128	19	Tang	25.37591 59.89553	29	Mangrove Gwadar	25.17594 61.47860
10	Khowr Jagin	25.59748 58.27522	20	Gurdim Bay	25.39829 60.06286	30	Khowr Bahokalat	25.20328 61.57267

2.2. Numerical Model Description

To assess the characteristics of waves in the Makran region, we have utilized the numerical model MIKE 21, which was developed by the Danish Hydraulic Institute (DHI) [25]. Although

various other numerical models, such as WAM [26], WW3 [27], SWAN [28], TOMAWAC [29], and ROMS [30], are available for simulating hydrodynamic conditions, MIKE 21 was selected due to its exceptional performance, comprehensive tools for data preparation and output analysis, and proven accuracy in numerous studies [12,13,31–35]. The MIKE 21 model is highly capable and widely employed for simulating wave and current characteristics in various environments, including river entrances, gulf interiors, coastal areas, as well as shallow and deep waters [11,12,26,31]. It is developed based on the fundamental principles of shallow water equations and the depth-integrated incompressible Reynolds averaged Navier-Stokes equations. The Spectral Waves (SW) module is designed to simulate the growth, decay, and transformation of wind-generated waves and swell in offshore and coastal areas. In this module, the waves are characterized using the density spectrum $N(\sigma,\theta)$, where σ represents the relative angular frequency ($\sigma = 2\pi f$) and θ represents the direction of wave propagation. The equation that governs the behavior of these waves is the wave action balance equation, which can be expressed in either cartesian or spherical coordinates (Eq. 1).

$$\frac{\partial N}{\partial t} + \nabla.(\vec{v}N) = \frac{s}{\sigma} \quad \rightarrow \frac{\partial}{\partial t}N + \frac{\partial}{\partial x}C_x N + \frac{\partial}{\partial y}C_y N + \frac{\partial}{\partial \sigma}C_\sigma N + \frac{\partial}{\partial \theta}C_\theta N = \frac{s}{\sigma} \tag{1}$$

where N represents the density of wave action, C_x, C_y, C_σ, and C_θ are parameters describing the velocity of the wave in geographical and spectral coordinate systems, and the term 's' represents the combination of five distinct energy sources, as described in Eq. 2.

$$s = s_{in} + s_{nl} + s_{ds} + s_{bot} + s_{surf} \tag{2}$$

In the context of energy generation, s_{in} represents the wind-generated energy, s_{nl} represents the transfer of wave energy resulting from the interaction between waves, s_{ds} accounts for the dissipation of wave energy caused by white capping, s_{bot} refers to the dissipation due to bottom friction, and s_{surf} represents the dissipation of wave energy resulting from breaking induced by changes in water depth [25,26,36].

Utilizing the spectral wave simulation feature within the MIKE 21 software package, spectral moments of order i are calculated using equation 3 to ascertain spectral wave parameters.

$$m_i = \int_0^{2\pi}\int_0^{\infty} E(f,\theta)\, f^i df\, d\theta, \tag{3}$$

where $E(f,\theta)$ denotes the directional wave energy spectrum, and f denote the wave frequency.

In the following, the key parameters associated with wave characteristics—namely, significant wave height (H_s), mean wave period (T_m), and energy period (T_e)—are determined using the following equations.

$$H_s = 4\sqrt{m_0} \tag{4}$$

$$T_m = \frac{m_0}{m_1} \tag{5}$$

$$T_e = \frac{m_{-1}}{m_0} \tag{6}$$

The wave power, denoted as the energy flux per unit crest length (P), is computed through the application of the directional wave power formulation, as expressed in Eq. 7.

$$\vec{P} = \rho g \int_0^{2\pi} \int_0^{\infty} \overrightarrow{C_g}(f,\theta)\, E\,(f,\theta) df\, d\theta, \quad (7)$$

where ρ, g and C_g are the density of seawater, the acceleration due to gravity, and group velocity respectively.

The wave power flux (P), in kW/m, can be calculated using Eq 8 [37,38].

$$P = \frac{\rho g^2}{64\pi} H_s^2 T_e \approx 0.49\, H_s^2 T_e, \quad (8)$$

2.3. Model Settings and Calibration

A mesh file prepared for the simulation comprising 6636 nodes and 10335 elements, and forming a flexible triangle. Three different mesh zone considered for the area (Fig. 2), where thinner mesh used for near shore area. The modeled area includes one land boundary (yellow line in Fig. 2), and three open boundaries of the eastern (green line in Fig. 2), the western (red line in Fig. 2), and the southern boundaries (blue line in Fig. 2). The bathymetric data is derived from the modified GEBCO data, and local nearshore data from Chabahar buoy (Fig 1C).

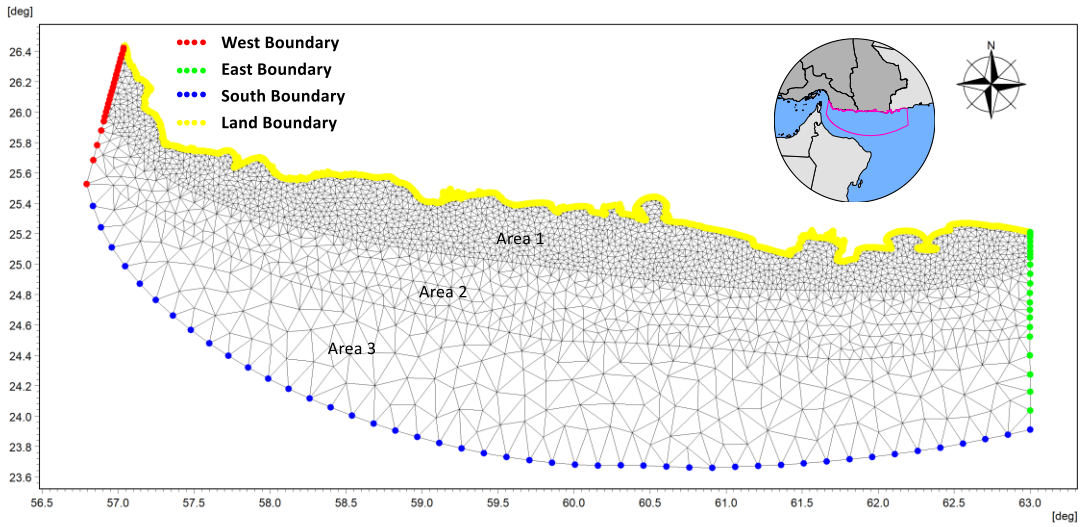


Figure 2. Mesh file with three open boundaries in the east (green), west (red) and south (blue)

Wind data obtained from European Centre for Medium-Range Weather Forecasts (ECMWF) ERA-40 [39] with a time step of 6 hours. The data is formatted as u and v components, with a spatial resolution of 0.125˚ × 0.125˚. (Fig. 3). According to the fig. 3 maximum wind speed is about 4 m/s. In the eastern part of the area, the prevailing wind direction is from the SE. In the central part, the wind speed is lower and predominantly originates from the E. In the western part, the prevailing wind direction is mostly from the NE.

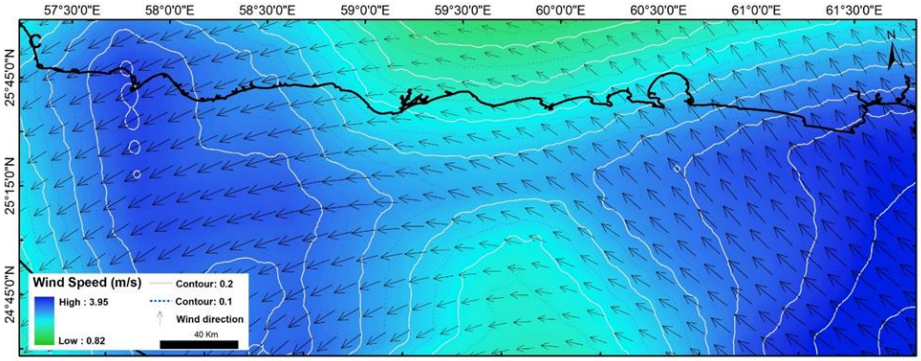


Figure 3. The Averaged wind speed and direction, of the year 2018, over the area, derived out from ECMWF ERA-40

Significant wave height (H_S), Spectral peak period (Tp), and Mean Wave Direction (MWD) are variables obtained from the ECMWF ocean model to utilize to the three open boundaries of the model. Initial conditions were set according to Anton et al., [40] and Ghaderi and Rahbani, [13] studies in the form of JONSWAP spectrum with a fetch of 100 km.

The calibration of the model involved the selection of specific coefficients related to wave breaking, bottom friction, and white capping parameters [12,13,31,40]. To optimize the results, various coefficient values were employed across multiple model iterations. Following extensive simulations and a thorough review of analogous studies, the selected parameters were: for wave breaking, Gamma was set to 0.8 and Alpha to 1; for bottom friction, Nikuradse roughness was set to 0.04; and for white capping, cdis was set to 4.5 and Delta to 0.05.

2.4. Model Validation

Following the enhancement of the model's performance, an evaluation was conducted, comparing H_S values simulated by MIKE 21 SW with those from the ECMWF ocean model data at the specified location illustrated in Fig. 2 (Fig. 4). Statistical parameters are imployed assess the quality of the model results [40,41]. The Correlation Coefficient (CC) [42] demonstrates a strong correlation between the patterns of both data series, with a value of 0.95. This parameter for the same region is reported as 0.98 by Ghaderi and Rahbani, [13]. The Root Mean Square Error (RMSE) [43] is calculated as 0.14, the Bias parameter (BIAS) [44] is derived as -0.02, and Dispersion Index (SI) [45] is computed as 13.8%. These statistical values implied that model results in this investigation are reliable.

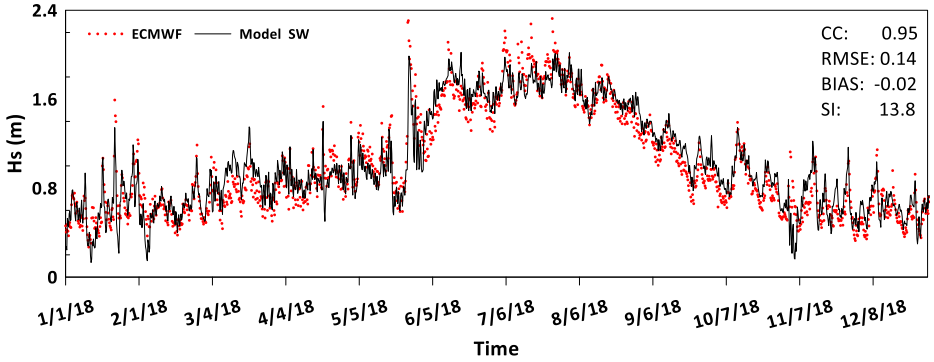


Figure 4. Comparison of the H_S obtained from the simulated MIKE 21 SW model and the ECMWF ocean model data in 2018

2.5. Fuzzy standardization and overlay

After completing the numerical model and obtaining the outputs from the spectral wave model, this study employs Fuzzy Logic to integrate the values of these variables in a comprehensive manner. This integration allows for a simultaneous consideration of all variables [35,46], thereby providing a detailed description of the wave patterns along the Makran coastline. We employed Fuzzy Logic [47] to combine the values of three variables, H_S, P, and MWD, to identify the sensivity of the region in response to the combination of these variables. Prior to the overlaying phase, it is necessary to standardize each variable, taking into account their diverse units and numerical ranges. In this study, standardization is achieved through the utilization of Fuzzy membership. Fuzzy membership assigns values to each variable within the range of zero to one, depending on the adopted concept [48–50].

In the sea and coastal zone, wave height serves as an indicative parameter of sea state [51], where higher fuzzy membership values signify a higher sea state. The variable H_S is standardized using the Linear function with the min and max values of 0 and 2.2m (highest observed value) respectively. Fig. 5 A illustrates annual average of H_S and corresponding fuzzy membership values within a one-km buffer from the Makran shoreline. Within this buffer, the maximum and average H_S are 1.06 and 0.58 m, respectively, yielding fuzzy membership values of 0.48 and 0.26 consequently (Table 2). Wave power denotes the rate of wave energy transfer (to the coast) [52], and regions with higher fuzzy membership values experience greater wave power. Increased wave power has the potential to increase erosion and flooding in coastal regions, while a substantial significant wave height indicates the presence of hazards and challenges in sea state [53,54]. Generally, greater wave height and a shorter wave period align with augmented risks and challenges in the sea state [55]. As a result, both variables are considered in this study. The P variable is subjected to standardization using the large function (midpoint=5, spread=5). The highest wave power value reaches up to 14 kW/m across the entire study area, primarily concentrated in the eastern part and during the summer period. Therefore, the midpoint of the large function is specified as 5. Fig. 5 B depicts the relationship between the annual average of P variable and the calculated fuzzy membership value within a one-km buffer from the shoreline. In this buffer, the maximum and average P values are 4.83 and 1.50 kW/m, respectively, resulting in fuzzy membership values of 0.46 and 0.04 consequently (Table 2). The MWD variable undergoes standardization through a Gaussian function (midpoint=180, spread=0.005). This standardization is based on the premise that waves approaching the coast at oblique angles are more likely to attack the coastal area [56,57]. Consequently, a reversal of the Gaussian function is required for this standardization. In this process, waves arriving from the southern side (180 degree) are assigned the lowest fuzzy membership value, while oblique waves receive the highest fuzzy membership value. Depicted in Fig. 5 C, the relationship between annual average of MWD and fuzzy membership (within a one-km shoreline buffer) is modeled using a Reverse Gaussian function. The mean is approximately 270° (StDev 17.6), with computed maximum and average fuzzy membership values of 1.0 and 0.66, respectively (Table 1).

Table 2. Annual average of Hs, P, and MWD variables for the year 2018 obtained from the output of the model and the standardized results through Fuzzy membership along the one-km buffer of Makran shoreline

Variable	Model output				Fuzzy membership				
	Min	Max	Mean	StDev*	Function	Min	Max	Mean	StDev
Hs	0.08	1.06	0.58	0.23	Liner	0.03	0.48	0.26	0.11
P	0.02	4.83	1.50	1.30	Large	0.00	0.46	0.04	0.09
MWD	106	269	196	17.63	Reverse Gaussian	0.00	1.00	0.66	0.31

*Standard deviation

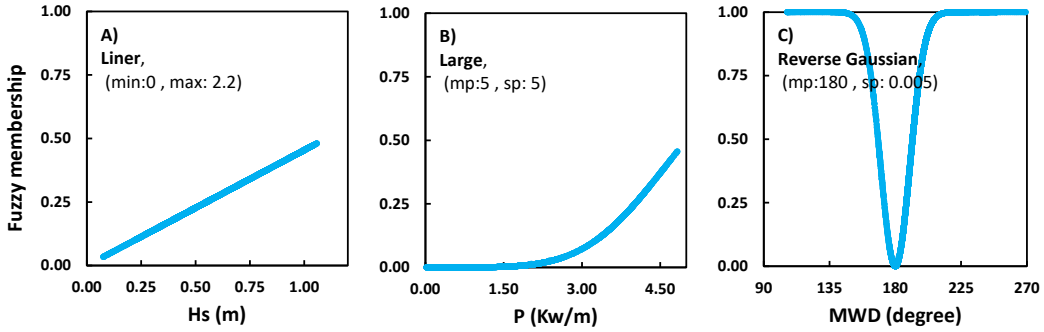


Figure 5. Annual averaged Hs, P, and MWD along the one-km buffer of Makran shoreline and their simultaneous fuzzy membership values (after standardized) through the introduced function.

To achieve overlaying, the fuzzy GAMMA operator was employed [58]. The principles of this operator are elucidated in Equation 9, encompassing both fuzzy sum and fuzzy product operators.

$$\mu_{Combination} = [1 - \prod_{i=1}^{n}(1-\mu_1)]^{\delta} \times \ [\prod_{i=1}^{n}\mu_1]^{1-\delta} \quad (9)$$

where, $\mu_{Combination}$ is the final result of the fuzzy combination, the μ_i is fuzzy value of each set i, δ is a weight parameter between 0 and 1, and, n is the number of fuzzy sets. The fuzzy GAMMA operator is governed by the δ parameter (gamma coefficient). Lower gamma coefficients mean low sensitivity class areas, while higher gamma coefficients signify areas with high sensitivity [59,60]. The selection of the δ parameter involves achieving a dynamic equilibrium between the impacts of augmenting and diminishing overlapping variables [59,61]. δ parameter should be chosen wisely in order to correctly signify the influence of combined parameter in the area. We employed the operator function for this reason. δ value of 0.9 has been selected to establish adaptable compatibility between escalating and diminishing trends.

3. Results and Discussion

3.1. Simulated variables

Considering the substantial variation in wave characteristics along the approximately 550 km Makran coast across different seasons, a brief overview of the seasonal conditions is first presented, followed by an explanation of the annual average results. The wave height (Hs) and wave power (P) along the Makran coast exhibit significant seasonal variations. In winter, the

eastern part faces higher H_S (up to 0.68 m) than the western part (less than 0.38 m), with coastal zones showing varying maximum H_S and P. Spring brings increased H_S and P, especially in the eastern regions, with H_S reaching up to 1.0 m and P up to 2.5 kW/m. Summer peaks with H_S up to 2.0 m in the east and maximum P reaching 13.5 kW/m in certain zones. Autumn sees a decline in H_S and P, resembling spring conditions, with H_S up to 1.0 m and P around 3.0 kW/m in the east. The direction of incoming waves shifts seasonally, primarily from the southwest in winter and spring, and from the south in summer and autumn (Table 3). Detailed illustrations and data for each season are provided in the appendix (A), with Fig. A1 to A4 depicting the averaged pattern of wave characteristics seasonally.

Table 3. Summary of seasonal variations in wave height (H_S) and wave power (P) along the makran coast

Season	Wave Height (H_S) (m)			Wave Power (P) (kW/m)			Wave Direction
	West	East	Notable Zones (Z)	West	East	Notable Zones (Z)	
Winter	< 0.38	0.68	Z 1-12: 0.36 m, Z 20-23: 0.4 m	Max: 0.45	Max: 1.0	Z 1-17: 0.45 kW/m, Z 17-28: 1.0 kW/m	Mainly SW, WSW in the west
Spring	< 0.48	1.0	Z 1-12: 0.52 m, Z 17-23: 0.78 m	Max: 0.65	Max: 2.5	Z 1-17: 0.65 kW/m, Z 17-28: 2.5 kW/m	Mainly SW, consistent with winter
Summer	2.0	< 0.80	Z 1-12: 0.84 m, Z 17-23: > 1.0 m	Max: 2.2	Max: 13.5	Z 1-10: 1.75 kW/m, Z 17-28: 13.5 kW/m	Mainly S, SW within the coastal zone
Autumn	< 0.5	1.0	Z 1-12: 0.60 m, Z 23-28: 0.94 m	Max: 1.0	Max: 3.0	Z 1-12: 1.0 kW/m, Z 19-28: 3.0 kW/m	Mainly S, similar to annual

Despite the existence of several studies on the Makran coast, a gap in detailed, region-specific data has remained. This study addresses this gap by focusing on coastal zones, analyzing H_S, P, and MWD data. The results illustrating the annual average wave pattern are presented in Fig. 6. In the eastern part, the maximal H_S reaches up to 1.2 m, while in the western part, it is under 0.6 m. Along the shoreline, from zone Bunji-ye Karbasi (1) to Gougsar (12), the maximum H_S is 0.60 m. Moving from zones Gougsar (12) to Kalāt (17), the maximal H_S increases to 0.78 m, and further east side from zone Kalāt (17) to Chahbahar (23) maximum H_S increases up to 0.87 m. Zones Chahbahar (23) to Pasabandar (28) encounter a maximal H_S of 1.0 m, whereas zones Pasabandar (28) to Khowr Bahokalat (30), situated in a deeper bay, experiences a maximal H_S of 0.8 m. The wave direction reveals two distinct zones, with the eastern part originating from the SbW direction and the western part from the SW direction. In coastal regions from zone Bunji-ye Karbasi (1) to Shahreni (8), the maximum P is 0.85 kW/m, escalating to 1.56 kW/m in zones Shahreni (8) to Khowr Galak (16), and peaking at 1.5 kW/m in zones Khowr Galak (16) to Pozm Bay (21). Zones Pozm Bay (21) to Chahbahar (23) exhibit a P surpassing 3.5 kW/m. Zones Chahbahar (23) to Beris (26) attain a maximal P of 4.5 kW/m, while zones Beris (26) to Pasabandar (28) reach a maximum of 5.2 kW/m. Finally, zones Pasabandar (28) to Khowr Bahokalat (30) register a P of less than 3.2 kW/m. These findings highlight a clear spatial variation in wave energy distribution along the Makran coast. This spatial heterogeneity suggests that coastal development and erosion mitigation strategies should be tailored to the specific wave dynamics of each region, particularly in the high-energy eastern zones where greater hydrodynamic forces pose increased risks to coastal

infrastructure. A notable example is the distinct hydrodynamic conditions at Beris Port, located in the eastern Makran region [12,13].

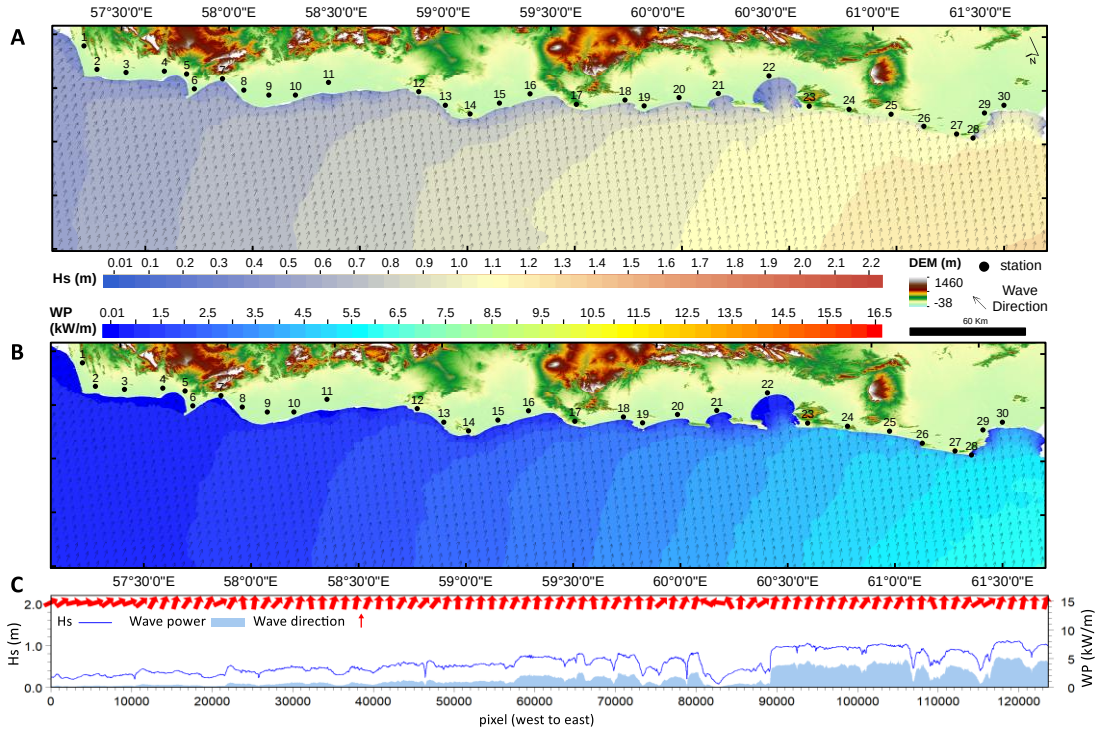


Figure 6. Annual pattern of A) averaged significant wave height, B) averaged wave power, and C) spatial variation diagram extracted from variables in a 1 km buffer from the Makran shoreline

To describe the temporal (seasonal and annual) variations of variables H_S, P, and MWD more specificly, box plots are used (Fig. 7 A-C). The spatial variations of H_S in the winter season are limited, ranging between 0.07 and 0.6 m, with an average of 0.4 m. During the spring season, H_S reached a maximum of 0.95 m with an average of 0.4 m, notably higher in the eastern half of the Makran region (Fig. A2, in Appendix). As the summer season commences, the most significant variations in H_S, up to 1.9 m with an average of 0.7 m, are observed throughout the entire area, with the eastern part experiencing higher H_S (Fig. A3, in Appendix). In the autumn season, H_S decreases, and the spatial variations in H_S resemble those in the spring season. The annual average spatial variations in H_S range from 0.08 to 1.1 m, with a mean of 0.5 m (Fig. 7A). The spatial and temporal variations in the variable P correspond to H_S (Fig. 7 B). The spatial variations of P in the spring season range from 0.0 to 1.08 kW/m, with a mean of 0.3 kW/m. In the summer season, spatial variations exceed 10.2 kW/m, with an average of 2.0 kW/m. The annual average spatial variations in P range from 0.02 to 5.3 kW/m, with a mean of 0.9 kW/m. Saket and Etemad-Shahidi, [62] conducted an investigation into the long-term wave power within zones Kalirak (14), Tang (19), Gurdim Bay (20), and Chabahar Bay (22), asserting that the monthly mean P fluctuates between 0.97 and 5.16 kW/m. Their findings are in concordance with the results of this study. In the spring season, the spatial variations of MWD range from 171 to 247 degrees, with an average of 208 degrees, and a similar pattern is observed in the spring, with the difference that directional dispersion increases. In the summer and autumn seasons, the pattern of spatial and temporal

variations in MWD is similar, with mean values of 191 and 189 degrees, respectively. Ghaderi and Rahbani's (2023) investigation also elucidates that the directional dispersion of waves along the coastal region exhibits greater diversity during the winter season in contrast to other temporal periods. The annual average spatial variations in MWD are within the range of 159 to 237 degrees, with a mean of 197 degrees (Fig. 7 C). The long-term analysis conducted by Saket and Etemad-Shahidi, [62] delineates the wave climate into three distinct temporal phases: the initial period spans from January to May, succeeded by a segment from June to August, and concluding with a phase spanning from September to December.

Since the area under investigation is faced with open ocean, the verity of winds are dominared in the area, which differes seasonally. At the onset of winter, wind speeds decrease, whereas during summer, the presence of the monsoon intensifies, leading to the formation of persistent southerly to southwesterly winds [19,62]. Consequently, the region's wave pattern is influenced by seasonal variations in wind, thus, the height, power and direction of waves are videly different season by season. These findings indicate that the distinct seasonal shifts in wave characteristics, particularly during the summer monsoon, can significantly affect sediment transport and coastal morphology. The variation in wave energy throughout the year suggests that coastal engineering solutions should be dynamic and flexible, taking into consideration not only the seasonal intensity of wave action but also the long-term impacts on shoreline stability and erosion patterns [63].

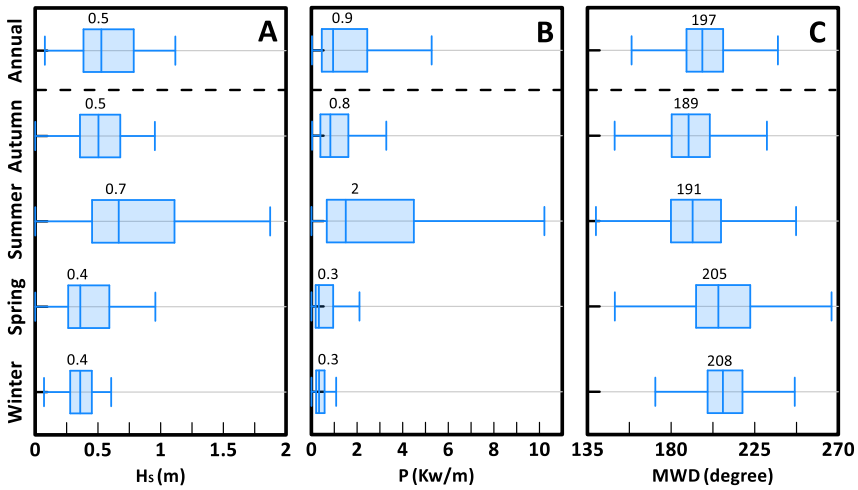


Figure 7. Box Plot of A) significant wave height, B) wave power, and C) mean wave direction (seasonally and annualy)

3.2. Overlaying variables

Overlaying three variables of H_S, P and MWD, the area were categorized and illustrated seasonally (Fig. 8 A-D), and annually (Fig. 8 E). During the spring season, the difference between the eastern and western regions is not pronounced, especially in coastal areas, which exhibit minimal conditions (Fig. 8 A). However, in the spring and summer seasons, the stark disparity and delineation of conditions between the eastern and western regions become highly evident (Fig. 8 B-C). This demarcation extends up to zone Kalāt (17) in the spring and penetrates up to zone 6 in the summer. In the autumn season, this demarcation reaches its maximum extent, up to zone Poshot (27) (Fig. 8 D). The results of overlaying the annual averages also indicate that this difference between the eastern and western sectors persists up to zone Kalāt (17). These findings highlight significant seasonal and spatial variations within the study area. Briefly, the eastern

region consistently exhibits higher scores compared to the western counterpart. The eastern region, adjacent to the Arabian Sea - Indian Ocean, is influenced by oceanic conditions and monsoon [11,19,64], while the western region is situated away from oceanic influences, there is a considerable reduction in depth, and the water body exhibits a semi-closed configuration.

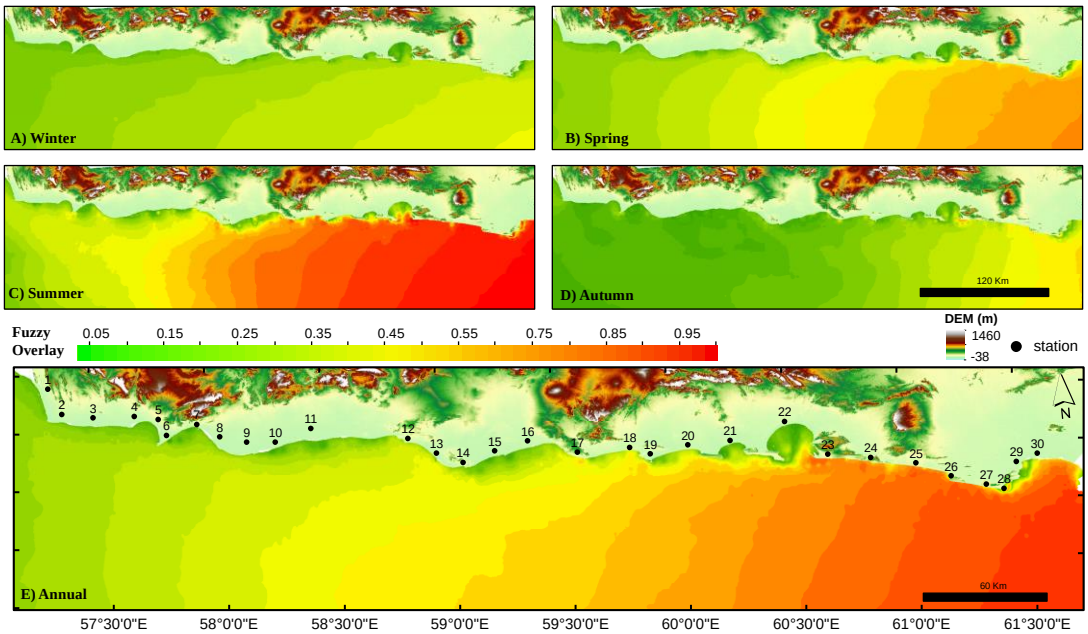


Figure 8. Overlaying outcomes of fuzzy layers (H_S, P, MWD) through the GAMMA method seasonally (A-D) and annually (E)

The seasonal and annual fluctuations of overlaying variables within a 1 km buffer from the shoreline are depicted in Fig. 9. The annual average overlaying variables score (black line in Fig. 9) reveals that zones Bunji-ye Karbasi (1) to Gougsar (12) exhibit scores below 0.4. Notably, from zone Kalirak (14) to Khowr Galak (16), intermediate zones Tang- Gurdim Bay (19-20), Gurdim Bay- Pozm Bay (20-21), zone Chabahar Bay (22), and zone Mangrove Gwadar (29) experience a discernible reduction attributed to the omega-shaped coast. Despite higher scores for the MWD variable in these regions, variables H_S and P register significantly lower scores (Fig. 9). Consequently, the overlayed variable indicate calm hydrodynamic conditions. In the western part, only a small segment of zones Lirak (13) and Kalāt (17) demonstrates overlaying variable scores surpassing 0.5. In these two areas, the wave enters with an oblique angle toward the shore (Fig. 6 C), resulting in a slight increase in the overall score of overlaying variables. In the eastern part, multiple regions exhibit annual average scores exceeding 0.5, such as zones Birdaf (18), Tang (19), Gurdim Bay (20), Pasabandar (28), and Khowr Bahokalat (30). Zones Birdaf, Gurdim Bay (20), and Khowr Bahokalat (30) represent open coastal areas, while zones Tang (19) and Pasabandar (29) constitute tombolo and capes, where waves with higher H_S and greater P exert influence. Between zones Chahbahar - Poshot (23-27), the overall score of annual average overlaying variables varies from 0.6 to 0.8. These coastal areas, characterized by highlands and rocky coasts, are fully exposed to oceanic conditions. Consequently, it is anticipated that the morphological response and coastal vulnerability in these regions to be significantly pronounced. In the study conducted by Siahsarani et al., [15], focusing on the investigation of the Gonu cyclone in the Gulf of Oman, it was articulated that a tropical cyclone has the potential to inflict damage,

both economic and environmental, to the coastal areas of Chabahar (the eastern zones in this study). Additionally, Ghaderi and Rahbani's [65] examination of the vulnerability of the eastern coast of Makran highlighted the susceptibility of these regions. These findings indicate that the high scores in eastern regions, influenced by oceanic conditions, may increase coastal vulnerability, highlighting the need for targeted management strategies to mitigate erosion and damage from extreme weather events.

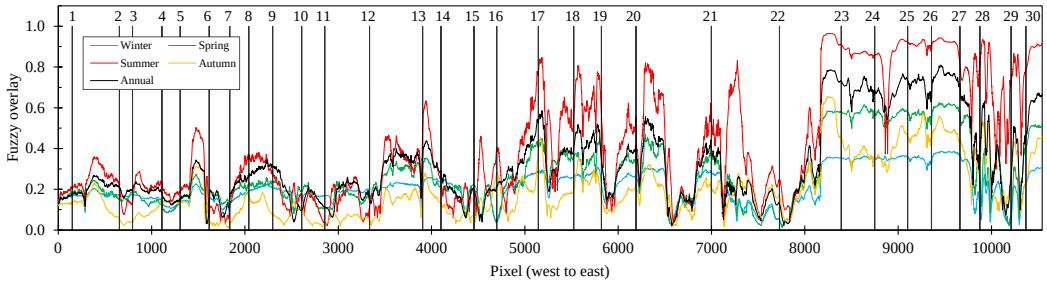


Figure 9. The results of overlaying fuzzy layers (H_S, P, MWD) using the GAMMA method, in a buffer of one km from Makran shore (The code for the indicator areas is provided at the top of the chart)

4. Conclusions

The primary objective of this study is to furnish detailed information on the wave patterns of the Makran coasts. Given the strategic importance of the Makran coasts for maritime development, a comprehensive understanding of their hydrodynamic conditions becomes essential. A numerical simulation was conducted to investigate the hydrodynamic conditions of the aera. The output results were utilized to analyze the seasonal and annual averages of wave height, wave power, and wave direction in the nearshore zone.For simultaneous analysis of variables, the data was subjected to Fuzzy Logic transformation using the fuzzy-GAMMA operator, and the values of all three variables were overlaid.

From a temporal perspective, the pattern of wave height and wave power can be categorized into three periods: winter and spring, characterized by minimal hydrodynamic conditions; summer, exhibiting maximum hydrodynamic conditions; and autumn, marking the onset of a decline in hydrodynamic conditions. The wave direction pattern in the nearshore zone falls into two periods: winter and spring, where the predominant wave direction is primarily south-southwest, and summer and autumn, where the waves are predominantly southern direction, besides the dispersion of directions within this timeframe is diverse. In terms of spatial variations, the hydrodynamic conditions are notably higher in the eastern section, particularly from the Kalāt zone to the Khowr Bahokalat zone, where both wave height and wave power are elevated, leading to increased coastal impact and erosion. Conversely, the western section generally exhibits lower hydrodynamic conditions, characterized by reduced wave height and wave power, resulting in less significant coastal effects. These variations are influenced by geographical features such as the coastline's orientation and bathymetric characteristics, which affect wave propagation and energy distribution. In the omega-shaped coast and bays, hydrodynamic conditions are generally minimal, except for the Gwadar Bay, which, due to its expansive entrance, experiences higher hydrodynamic conditions compared to other bays. The results of overlaying variable scores indicate that the hydrodynamic conditions in the coastal zone align with the analysis of temporal and spatial patterns of wave height and wave power. However, in certain locations such as

headlands, and capes, the hydrodynamic conditions have increased due to the oblique angle of waves in the nearshore zone.

Key findings include:

- **Wave Height (H_S):** Ranges from 0.07 to 1.9 m, peaking during summer with an average of 0.7 m. Winter and spring show calmer conditions with an average HS of 0.4 m. This parameter serves as an indicator of sea state and is crucial for understanding potential impacts on coastal infrastructure and erosion.
- **Wave Power (P):** Shows significant seasonal variation, with a marked increase in summer, reaching up to 10.2 kW/m, and an annual mean ranging from 0.02 to 5.3 kW/m. Increased wave power can lead to enhanced erosion and flooding risks, necessitating careful consideration in coastal development planning.
- **Wave Direction (MWD):** Exhibits seasonal variation, primarily ranging from 171° to 247° during winter and spring, and from 189° to 191° in summer and autumn. Waves approaching from the southern direction (180 degrees) exert minimal impact on the coastline, whereas oblique waves have a more pronounced effect, influencing coastal sediment transport and erosion patterns.

The findings of this study, along with similar studies, will assist planners and policymakers in developing management goals for coastal development. By integrating hydrodynamic dynamics into coastal planning, resilient strategies can be established for the sustainable utilization of the Makran region's resources, balancing maritime potential with risk mitigation.

Appendix

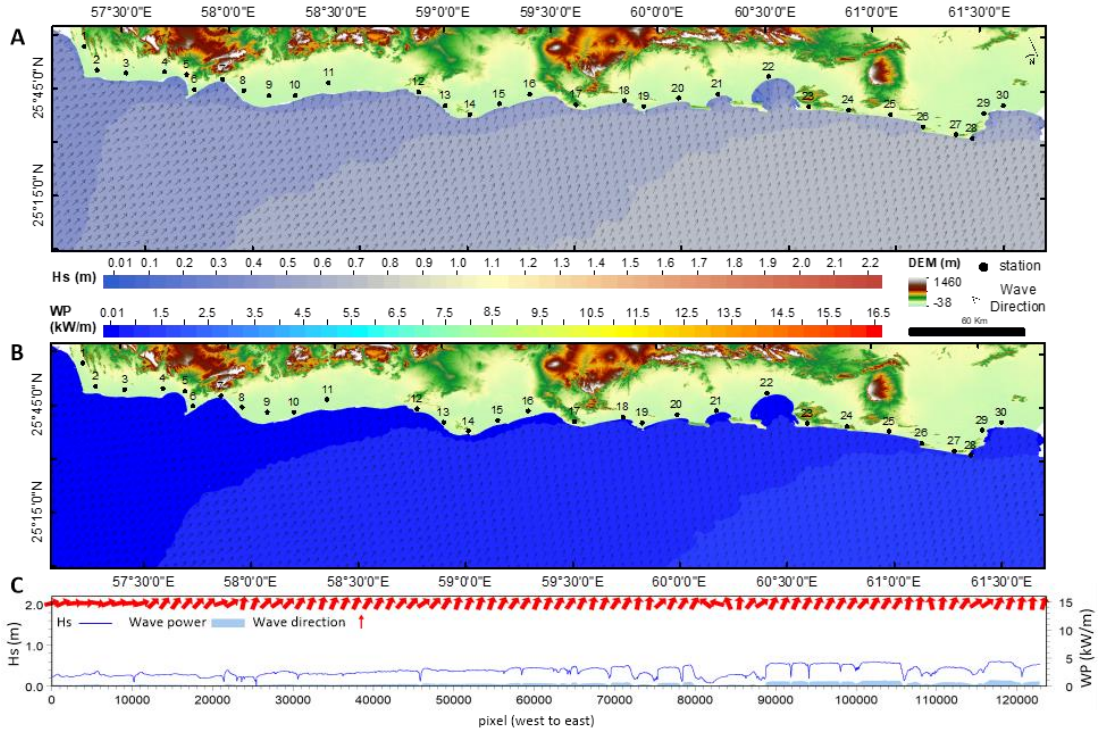


Figure A1: Winter season; Pattern of A) averaged significant wave height, B) averaged wave power, and C) spatial variation diagram extracted from variables in a 1 km buffer from the Makran shoreline

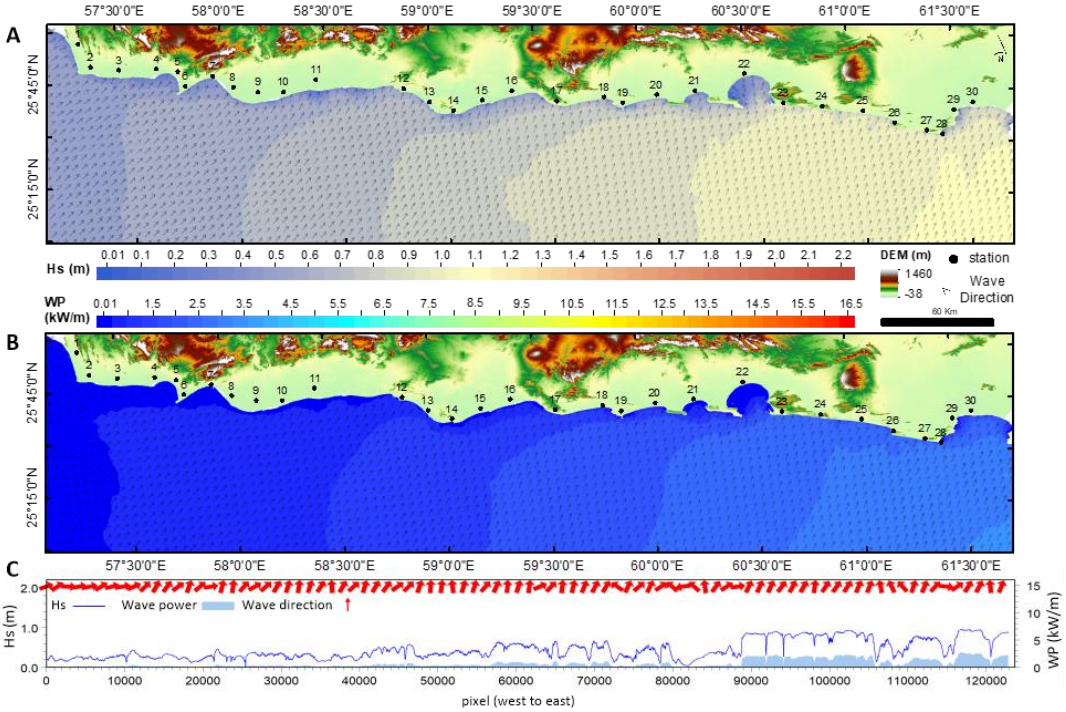


Figure A2: Spring season; Pattern of A) averaged significant wave height, B) averaged wave power, and C) spatial variation diagram extracted from variables in a 1 km buffer from the Makran shoreline

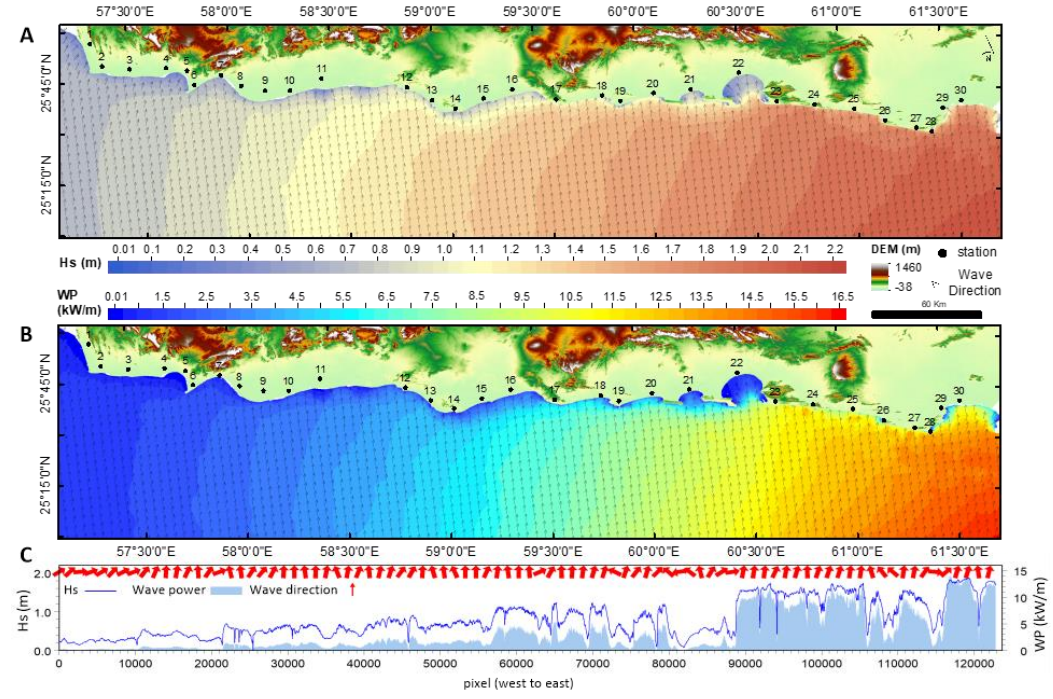


Figure A3: Summer season; Pattern of A) averaged significant wave height, B) averaged wave power, and C) spatial variation diagram extracted from variables in a 1 km buffer from the Makran shoreline

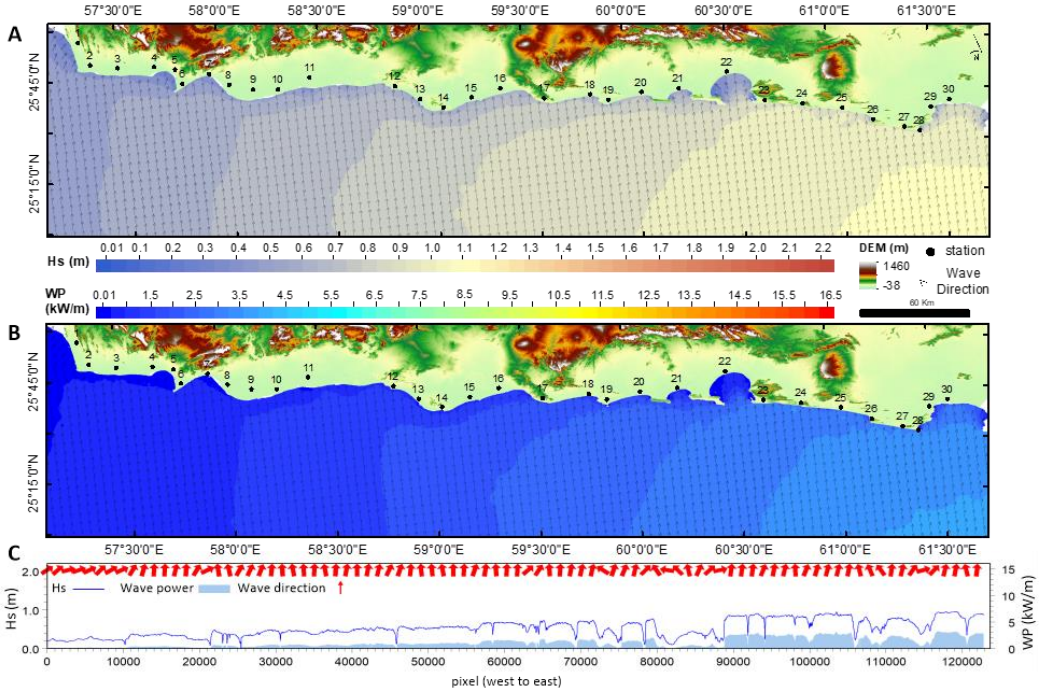


Figure A4: Autumn season; Pattern of A) averaged significant wave height, B) averaged wave power, and C) spatial variation diagram extracted from variables in a 1 km buffer from the Makran shoreline

References

1. United Nations. (2017). Factsheet: People and oceans. In Proceedings of the Ocean Conference (pp. 1–7).
2. Stewart, R. H., Introduction to physical oceanography, 2008.
3. Boye, C. B., Appeaning Addo, K., Wiafe, G., & Dzigbodi-Adjimah, K, (2018). Spatio-temporal analyses of shoreline change in the Western Region of Ghana. Journal of Coastal Conservation, 22(4), 769–776. DOI: 10.1007/s11852-018-0607-z
4. Church, J., Wilson, S., Woodworth, P., & Aarup, T, (2007). Understanding sea level rise and variability. Eos, Transactions American Geophysical Union, 88(4), 43–43. DOI: 10.1029/2007EO040008
5. Bird, E. C. F., Coastal geomorphology: an introduction. John Wiley Sons, 2008
6. Passeri, D. L., Hagen, S. C., Medeiros, S. C., Bilskie, M. V., Alizad, K., & Wang, D. (2015). The dynamic effects of sea level rise on low-gradient coastal landscapes: A review. Earth's Future, 3(6), 159–181. DOI: 10.1002/2015EF000298
7. Ye, X., & Niyogi, D, (2022). Resilience of human settlements to climate change needs the convergence of urban planning and urban climate science. Computational Urban Science, 2(1), 6. DOI: 10.1007/s43762-022-00035-0
8. Savastano S, Gomes da Silva P, Sánchez JM, Tort AG, Payo A, Pattle ME, Garcia-Mondéjar A, Castillo Y, Monteys X, (2024). Assessment of Shoreline Change from SAR Satellite Imagery in Three Tidally Controlled Coastal Environments. Journal of Marine Science and Engineering, 12(1), 163. DOI: 10.3390/jmse12010163.

9. Akbarian, M., & Khoorani, A, (2022). The impacts of climate variability on the wind erosion potentials: western region of Makran coastal plain, South of Iran. Theoretical and Applied Climatology, 149(3–4), 1209–1221. DOI:10.1007/s00704-022-04094-5
10. Allahdadi, M. N., Chaichitehrani, N., Allahyar, M., & McGee, L, (2017). Wave Spectral Patterns during a Historical Cyclone: A Numerical Model for Cyclone Gonu in the Northern Oman Sea. Open Journal of Fluid Dynamics, 07(02), 131–151. DOI:10.4236/ojfd.2017.72009
11. Moghaddam, E. I., Allahdadi, M. N., Hamedi, A., & Nasrollahi, A, (2018). Wave-induced currents in the northern Gulf of Oman: a numerical study for Ramin Port along the Iranian coast. American Journal of Fluid Dynamics, 8(1), 30–39. DOI:10.5923/j.ajfd.20180801.04
12. Sayehbani, M., Ghaderi, D, (2019). Numerical Modeling of Wave and Current Patterns of Beris Port in East of Chabahar-Iran. International Journal Of Coastal, Offshore And Environmental Engineering, 3(1), 21–29. DOI: 10.22034/ijcoe.2019.149314
13. Ghaderi, D., & Rahbani, M, (2023). Simultaneous employment of hydrodynamical simulation and RS imageries for analyzing the influence of an anthropogenic construction on shoreline transformation. Journal of Hydraulic Structures, 9(3), 14–31. DOI: 10.22055/jhs.2023.44699.1262
14. Armanfar, M., Goharnejad, H., Niri, M. Z., & Perrie, W, (2019). Assessment of coastal vulnerability in Chabahar Bay due to climate change scenarios. Oceanologia, 61(4), 412–426. DOI:10.1016/j.oceano.2019.03.001
15. Siahsarani, A., Karami Khaniki, A., Aliakbari Bidokhti, A.-A., & Azadi, M, (2021). Numerical Modeling of Tropical Cyclone-Induced Storm Surge in the Gulf of Oman Using a Storm Surge–Wave–Tide Coupled Model. Ocean Science Journal, 56(3), 225–240. DOI: 10.1007/s12601-021-00027-x
16. Foroutani, R., Rahbani, M., & Pakhirehzan, M, (2018). Investigating the Storm Surge Due to Tropical Cyclone Ashobaa in the Coastal Areas of Bushehr and Chabahar. Journal of Oceanography, 8(32), 9–19. DOI: 10.29252/joc.8.32.9
17. Ghanavati, E., Shah-Hosseini, M., Marriner, N. (2021). Analysis of the Makran Coastline of Iran's Vulnerability to Global Sea-Level Rise. Journal of Marine Science and Engineering, 9(8), 891. DOI: 10.3390/jmse9080891
18. Hafeznia M.R, Alamdar E., Rezaei Seke Ravani D, (2020). The Role of Developing the Makran Coast and Iran's Marine Orienteering Strategy on the Development of the Eastern Axis of the Country. Political Organizing of Space, 2(2).
19. Chaichitehrani, N., & Allahdadi, M. N. (2018). Overview of wind climatology for the Gulf of Oman and the northern Arabian Sea. American Journal of Fluid Dynamics, 8(1), 1–9. DOI: 10.5923/j.ajfd.20180801.01
20. Pous, S. P., Carton, X., & Lazure, P, (2004). Hydrology and circulation in the Strait of Hormuz and the Gulf of Oman—Results from the GOGP99 Experiment: 2. Gulf of Oman. Journal of Geophysical Research: Oceans, 109(C12). DOI: 10.1029/2003JC002146
21. Rashidi, A., Dutykh, D., Shomali, Z. H., Keshavarz Farajkhah, N., & Nouri, M. (2020). A Review of Tsunami Hazards in the Makran Subduction Zone. Geosciences, 10(9), 372. DOI: 10.3390/geosciences10090372

22. Salah, P., Sasaki, J., & Soltanpour, M, (2021). Comprehensive Probabilistic Tsunami Hazard Assessment in the Makran Subduction Zone. Pure and Applied Geophysics, 178(12), 5085–5107. DOI: 10.1007/s00024-021-02725-y
23. Pourkerman, M., Marriner, N., Hamzeh, M.-A., Lahijani, H., Morhange, C., Amjadi, S., et al. (2022). Socioeconomic impacts of environmental risks in the western Makran zone (Chabahar, Iran). Natural Hazards, 112(2), 1823–1849. DOI: 10.1007/s11069-022-05230-0
24. He, W., Liu, J., Huang, Y., & Cao, L, (2020). Sea Level Change Controlled the Sedimentary Processes at the Makran Continental Margin Over the Past 13,000 yr. Journal of Geophysical Research: Oceans, 125(3). DOI: 10.1029/2019JC015703
25. Group-DHI. (2017). MIKE 21 Spectral Wave Module, Scientific Documentation. Hørsholm, Denmark: DHI Water Environment Health.
26. Komen, G. J., Cavaleri, L., Donelan, M., Hasselmann, K., Hasselmann, S., & Janssen, P, Dynamics and modelling of ocean waves, 1996. DOI: 10.1017/CBO9780511628955
27. Tolman HL. (2009). User manual and system documentation of WAVEWATCH III TM version 3.14. Technical note, MMAB contribution.;276(220).
28. Delft, T. (2014). SWAN User Manual Cycle III version 41.01. Delft, Nederlands: Delft University of Technology Faculty of Civil Engineering and Geosciences Environmental Fluid Mechanics Section.
29. TOMAWAC. (2014). TOMAWAC wave model.
30. Moore, AM., Arango, HG., Broquet, G., Edwards, C., Veneziani, M., Powell, B., et al. (2011). The Regional Ocean Modeling System (ROMS) 4-dimensional variational data assimilation systems. Progress in Oceanography. 91(1):50–73. DOI: 10.1016/j.pocean.2011.05.004
31. Pakhirehzan, M., Rahbani, M., & Malakooti, H. (2018). Numerical Study of Winter Shamal Wind Forcing on the Surface Current and Wave Field in Bushehr's Offshore Using MIKE21. International Journal of coastal and offshore engineering, 2(2), 57–65. DOI: 10.29252/ijcoe.2.2.57
32. Wu, C., Wan, J., Wang, Y., Bi, Z., Wang, Y., Ren, X. (2024). Evaluation of water quality fluctuation in the tidal reach under the impact of on shore wastewater discharges based on MIKE 21 model in Dongguan, China. Physics and Chemistry of the Earth, Parts A/B/C. 103730. DOI: 10.1016/j.pce.2024.103730
33. Upadhyaya, S., Rao, S., Rao, M. (2024). Assessment of wind and wave energy potential along the Indian coast. Cogent Engineering. 31;11(1). DOI: 10.1080/23311916.2024.2316950
34. Djili, M., Mezouar, K., Benaissa, N. (2024). Wave Climate, Sediment Transport and Shoreline Evolution in the West Littoral of Algeria. Ocean Science Journal. 28;59(3):39. DOI: 10.1007/s12601-024-00165-y
35. Ghaderi, D. (2024). Mapping the shoreline risk assessment of oil spill in the eastern region of Qeshm channel. Marine Pollution Bulletin. 206:116714. DOI: 10.1016/j.marpolbul.2024.116714
36. Remya, P. G., Kumar, R., & Basu, S. (2014). An assessment of wind forcing impact on a spectral wave model for the Indian Ocean. Journal of Earth System Science, 123(5), 1075–1087. DOI: 10.1007/s12040-014-0450-z

37. Jadidoleslam, N., Özger, M., & Ağıralioğlu, N, (2016). Wave power potential assessment of Aegean Sea with an integrated 15-year data. Renewable Energy, 86, 1045–1059. DOI: 10.1016/j.renene.2015.09.022
38. Abdollahzadehmoradi, Y., Özger, M., & Altunkaynak, A, (2018). Long-Term Macro-Scale Assessment of Wave Power of Black Sea by an Optimized Numerical Model. Iranian Journal of Science and Technology, Transactions of Civil Engineering, 42(4), 391–414. DOI: 10.1007/s40996-018-0108-1
39. Uppala, S. M., KÅllberg, P. W., Simmons, A. J., Andrae, U., Bechtold, V. D. C., Fiorino, M., et al. (2005). The ERA-40 re-analysis. Quarterly Journal of the Royal Meteorological Society, 131(612), 2961–3012. DOI: 10.1256/qj.04.176
40. Anton, I. A., Rusu, L., Anton, C., Anton, Rusu, & Anton, (2019). Nearshore wave dynamics at Mangalia beach simulated by spectral models. Journal of Marine Science and Engineering, 7(7), 206. DOI:10.3390/jmse7070206
41. Mahmoodi, A., Lashteh Neshaei, M. A., Mansouri, A., & Shafai Bejestan, M, (2020). Study of Current- and Wave-Induced Sediment Transport in the Nowshahr Port Entrance Channel by Using Numerical Modeling and Field Measurements. Journal of Marine Science and Engineering, 8(4), 284. DOI: 10.3390/jmse8040284
42. Kalra, R., & Deo, M. C. (2007). Derivation of coastal wind and wave parameters from offshore measurements of TOPEX satellite using ANN. Coastal Engineering, 54(3), 187–196. DOI: 10.1016/j.coastaleng.2006.07.001
43. Cox, A. T., & Swail, V. R. (2001). A global wave hindcast over the period 1958--1997: Validation and climate assessment. Journal of Geophysical Research, 106(C2), 2313–2329. DOI: 10.1029/2001JC000301
44. Mahjoobi, J., Etemad-Shahidi, A., & Kazeminezhad, M. H, (2008). Hindcasting of wave parameters using different soft computing methods. Applied Ocean Research, 30(1), 28–36. DOI: 10.1016/j.apor.2008.03.002
45. Rusu, E. (2018). An analysis of the storm dynamics in the Black Sea. The Romanian Journal of Technical Sciences. Applied Mechanics, 63, 131–146.
46. Dávila-Lamas, AD., Carbajal-Hernández, JJ., Sánchez-Fernández, LP., Niebla-Zatarain, VB., Hoil-Rosas, CA. (2022). Assessment of Coastal Locations Safety Using a Fuzzy Analytical Hierarchy Process-Based Model. Sustainability. 14;14(10):5972. DOI: 10.3390/su14105972
47. Zadeh, L. A. (1996). FUZZY SETS (pp. 394–432). DOI: 10.1142/9789814261302_0021
48. Tabrizi, N., Taghvaei, M., & Varesi, H. R, (2012). A fuzzy application on MICE hosting: An Iranian case study for locating suitable areas based on P.L Indexes. Management Science Letters, 2(2), 503–510. DOI: 10.5267/j.msl.2011.12.024
49. Ghadamode, V., Srivastava, K., Singh, R. K., & Pandey, A. K, (2022). Spatial analysis techniques for tsunami vulnerability and inundation mapping of Andaman region using remote sensing, GIS, AHP, and Fuzzy logic methods. Environmental Earth Sciences, 81(17), 427. DOI: 10.1007/s12665-022-10548-w

50. Lee, S. (2007). Application and verification of fuzzy algebraic operators to landslide susceptibility mapping. Environmental Geology, 52(4), 615–623. DOI: 10.1007/s00254-006-0491-y
51. Obakrim, S., Ailliot, P., Monbet, V., & Raillard, N, (2023). Statistical modeling of the space–time relation between wind and significant wave height. Advances in Statistical Climatology, Meteorology and Oceanography, 9(1), 67–81. DOI: 10.5194/ascmo-9-67-2023
52. Falnes, J, (2007). A review of wave-energy extraction. Marine Structures, 20(4), 185–201. DOI: 10.1016/j.marstruc.2007.09.001
53. Ozkan, C., Perez, K., & Mayo, T. (2020). The impacts of wave energy conversion on coastal morphodynamics. Science of The Total Environment, 712, 136424. DOI: 10.1016/j.scitotenv.2019.136424
54. Ozkan, C., Mayo, T., & Passeri, D. L, (2022). The Potential of Wave Energy Conversion to Mitigate Coastal Erosion from Hurricanes. Journal of Marine Science and Engineering, 10(, 143. DOI: 10.3390/jmse10020143
55. Chaigneau, A. A., Law-Chune, S., Melet, A., Voldoire, A., Reffray, G., & Aouf, L, (2023). Impact of sea level changes on future wave conditions along the coasts of western Europe. Ocean Science, 19(4), 1123–1143. DOI: 10.5194/os-19-1123-2023
56. Falqués, A., Calvete, D., & Ribas, F, (2011). Shoreline Instability due to Very Oblique Wave Incidence: Some Remarks on the Physics. Journal of Coastal Research, 27(2), 291. DOI: 10.2112/JCOASTRES-D-09-00095.1
57. Ashton, A. D., & Murray, A. B, (2006). High-angle wave instability and emergent shoreline shapes: 2. Wave climate analysis and comparisons to nature. Journal of Geophysical Research: Earth Surface, 111(F4). DOI: 10.1029/2005JF000423
58. Bonham-Carter, G, Geographic information systems for geoscientists: modelling with GIS. Elsevier, 1994. DOI: 10.1016/C2013-0-03864-9
59. Moradpanah, M., Monavari, S. M., Shariat, S. M., Khan Mohammadi, M., & Ghajar, I, (2022). Evaluation of Ecological Vulnerability of Coasts of the Caspian Sea Based on Multi-criteria Decision Methods (Iran). Journal of the Indian Society of Remote Sensing, 50(12), 2479–2502. DOI: 10.1007/s12524-022-01612-w
60. Vafai, F., Hadipour, V., & Hadipour, A, (2013). Determination of shoreline sensitivity to oil spills by use of GIS and fuzzy model. Case study – The coastal areas of Caspian Sea in north of Iran. Ocean & Coastal Management, 71, 123–130. DOI: 10.1016/j.ocecoaman.2012.05.033
61. Sadeghi, B., & Khalajmasoumi, M. (2015). A futuristic review for evaluation of geothermal potentials using fuzzy logic and binary index overlay in GIS environment. Renewable and Sustainable Energy Reviews, 43, 818–831. DOI: 10.1016/j.rser.2014.11.079
62. Saket, A., Etemad-Shahidi, A, (2012). Wave energy potential along the northern coasts of the Gulf of Oman, Iran. Renewable Energy, 40(1), 90–97. DOI: 10.1016/j.renene.2011.09.024
63. Srinivas, G., Remya, PG., Malavika, S., Nair TMB. (2020). The influence of boreal summer intra-seasonal oscillations on Indo-western Pacific Ocean surface waves. Scientific Reports. 28;10(1):12631. DOI: 10.1038/s41598-020-69496-9

64. Chitrakar, P., Baawain, M. S., Sana, A., & Al-Mamun, A, (2020). Hydrodynamic measurements and modeling in the coastal regions of Northern Oman. Journal of Ocean Engineering and Marine Energy, 6(2), 99–119. DOI: 10.1007/s40722-020-00161-z
65. Ghaderi, D., & Rahbani, M, (2024). Evaluating the shoreline vulnerability of eastern coast of Makran employing geomorphological and hydrodynamic parameters. Journal of Earth System Science, 133(2), 48. DOI: 10.1007/s12040-024-02266-7

© 2025 by the authors. Licensee SCU, Ahvaz, Iran. This article is an open access article distributed under the terms and conditions of the Creative Commons Attribution 4.0 International (CC BY 4.0 license) (http://creativecommons.org/licenses/by/4.0/).